

PCCP

Accepted Manuscript



This is an *Accepted Manuscript*, which has been through the Royal Society of Chemistry peer review process and has been accepted for publication.

Accepted Manuscripts are published online shortly after acceptance, before technical editing, formatting and proof reading. Using this free service, authors can make their results available to the community, in citable form, before we publish the edited article. We will replace this *Accepted Manuscript* with the edited and formatted *Advance Article* as soon as it is available.

You can find more information about *Accepted Manuscripts* in the [Information for Authors](#).

Please note that technical editing may introduce minor changes to the text and/or graphics, which may alter content. The journal's standard [Terms & Conditions](#) and the [Ethical guidelines](#) still apply. In no event shall the Royal Society of Chemistry be held responsible for any errors or omissions in this *Accepted Manuscript* or any consequences arising from the use of any information it contains.

**Phonon-assisted energy back transfer-induced multicolor
upconversion emission of $\text{Gd}_2\text{O}_3:\text{Yb}^{3+}/\text{Er}^{3+}$ nanoparticles under
near-infrared excitation**

Jun Liu, Huawei Deng, Yueli Zhang, DiHu Chen*, Yuanzhi Shao*

State Key Laboratory of Optoelectronic Materials and Technologies, Sun Yat-sen
University, Guangzhou 510275, P.R. China

* Corresponding authors. E-mail: stscdh@mail.sysu.edu.cn; stssyz@mail.sysu.edu.cn.

Mobile: 86-20-13600452080, Fax: 86-20-84113398.

Abstract: Manipulation of upconversion (UC) emission is of particular importance for multiplexed bioimaging. Here, we precisely manipulate the UC color output by utilizing the phonon-assisted energy back transfer (EBT) process in ultra-small (sub-10 nm) $\text{Gd}_2\text{O}_3:\text{Yb}^{3+}/\text{Er}^{3+}$ UC nanoparticles (UCNPs). We synthesized the $\text{Gd}_2\text{O}_3:\text{Yb}^{3+}/\text{Er}^{3+}$ UCNPs by adopting the laser ablation in liquids (LAL) technique. The synthesized $\text{Gd}_2\text{O}_3:\text{Yb}^{3+}/\text{Er}^{3+}$ UCNPs are small spherical and monoclinic structures. Continuous color-tunable (from green to red) UC fluorescence emission is achieved by increasing the concentration of Yb^{3+} ions from 0 to 15 mol%. A phonon-assisted energy back transfer (EBT) process from Er^{3+} ($^4S_{3/2} \rightarrow ^4I_{13/2}$) to nearby Yb^{3+} ($^2F_{7/2} \rightarrow ^2F_{5/2}$), which can significantly enhance red emission at 672 nm and decrease green emission, is responsible for the color-tunable UC emission by increasing the Yb^{3+} concentration in $\text{Gd}_2\text{O}_3:\text{Yb}^{3+}/\text{Er}^{3+}$ UC nanoparticles.

Key words: Upconversion nanoparticles; Multicolor emission; Energy back transfer; Multiphonon relaxation; Cross relaxation

1. Introduction

Lanthanide-doped upconversion nanoparticles (UCNPs) are a promising new generation of fluorescence nanoprobes in biological imaging.¹⁻³ For practical purposes, there is no doubt that the multicolor nanoprobes will play a vital role in diagnosing diseases in the near future. The multicolor nanoprobes can be applied for multiplexed bioimaging, which not only enables real-time imaging and tracking of multiple targets simultaneously, but also allows scientists to understand, classify, and differentiate complex human diseases.⁴⁻¹⁰ Thus, the manipulation of upconversion (UC) emission is of particular importance. Many strategies have been devoted to designing and tuning the UC emission, and include selecting different sensitizer/activator combinations or their concentrations,¹¹⁻¹⁴ utilization of appropriate energy transfer or migration pathways,¹⁵ and controlling the relaxation processes.¹⁶⁻¹⁸ The main mechanism (nonradiative energy transfer) of UC involves fundamental multipolar and/or exchange interaction between two lanthanide ions, which are strongly dependent on the average ion-ion distance.¹⁹ Thus, the selection of different sensitizer/activator combinations or their concentrations is a straightforward and useful approach to tune the multicolor emission. However, a high concentration of dopant ions can introduce luminescence quenching.²⁰ To the best of our knowledge, the concentration of the activator ions (e.g., Er^{3+} , Ho^{3+} , and Tm^{3+}) in UCNPs is usually constrained below 2 mol%, and the concentration of the sensitizer (Yb^{3+}) is constrained below 20 mol%.^{21, 22}

Fluorides and oxides are most frequently used as host materials. Fluorides have

attracted much attention and exhibit high UC efficiency due to their low phonon energy, and UC multicolor fine-tuning based on different sensitizer/activator combinations or their concentrations in the fluorides has been achieved by several groups.²²⁻²⁵ Nonetheless, the toxicity of fluorine must be concerned for biomedical applications. Compared with fluorides, oxides are more suitable for biomedical applications due to their lower toxicity and desirable chemical stability.²⁶ However, the ability of oxides to regulate the UC multicolor emission output with slight doping is often overlooked, because the phonon energy of the oxide matrices is higher than the fluorides, which is often perceived as deleterious.²¹ Despite this, it should be noted that the UC fluorescence can be effectively tuned by slightly changing the dopants concentration in oxides matrices.²⁷⁻³⁰ Lojpur et al. obtained visible green, yellow, and red fluorescence by doping with 1, 2.5, and 5 mol% Yb^{3+} ions in $\text{Y}_2\text{O}_3:\text{Yb}^{3+}/\text{Er}^{3+}$ nanoparticles.³¹ Green and red fluorescence have been obtained by doping with 0 and 10 (or 15) mol% Yb^{3+} ions in $\text{Gd}_2\text{O}_3:\text{Yb}^{3+}/\text{Er}^{3+}$ nanomaterials.^{32,33} However, the UC emission in these studies are relative monotonic without reflecting the fine-tuning capability of dopants in oxide hosts. More importantly, we still need a comprehensive understanding of the fluorescence-tuning mechanism.

Our previous work has demonstrated that the lanthanide doped small Gd_2O_3 nanoparticles synthesized by laser ablation in liquid (LAL) have great potential in bioimaging applications.³⁴⁻³⁶ In this work, we investigate the sensitizer (Yb^{3+}) concentration-dependent multicolor UC emission in small-sized monoclinic $\text{Gd}_2\text{O}_3:\text{Yb}^{3+}/\text{Er}^{3+}$ UCNPs. We illuminate eye-compatible and continuously

color-tunable fluorescence (from green to red) via adjusting the Yb^{3+} concentration (from 0 to 15 mol%) in $\text{Gd}_2\text{O}_3:\text{Yb}^{3+}/\text{Er}^{3+}$ UCNPs. The UC mechanism for fluorescence tuning is also discussed systematically based on the experimental results and steady-state rate equations.

2. Results and discussion

The UC process employs invisible NIR light (980 nm) excitation to produce visible fluorescence (Fig. 1a). Digital fluorescence images of the as-prepared $\text{Gd}_2\text{O}_3:\text{Yb}^{3+}(x \text{ mol}\%, x=0, 2, 5, 10, \text{ and } 15)/\text{Er}^{3+}(2 \text{ mol}\%)$ UCNPs colloids are shown in Fig. 1b. These images are recorded by a digital camera under excitation at 980 nm without using any optical filters. Clearly, continuous visible fluorescence from green to red (left to right) is observed with the increase of Yb^{3+} concentrations from 0 to 15 mol%. The multicolor emissions of UCNPs are naked-eye compatible and reflect their real fluorescence colors.

The crystal structures of the $\text{Gd}_2\text{O}_3:\text{Yb}^{3+}/\text{Er}^{3+}$ UCNPs were characterized by XRD measurement. The as-prepared UCNPs colloids are doped on silicon substrates and evaporated for measurement. The XRD patterns of $\text{Gd}_2\text{O}_3:\text{Yb}^{3+}/\text{Er}^{3+}$ UCNPs shown in Fig. 2 match well with the monoclinic Gd_2O_3 (PDF#42-1465), which suggests that the different doping concentrations of Yb^{3+} do not change the monoclinic structure of the Gd_2O_3 in these nanoparticles.

The morphology of $\text{Gd}_2\text{O}_3:\text{Yb}^{3+}/\text{Er}^{3+}$ UCNPs has no obvious difference. The typical TEM image (take $\text{Gd}_2\text{O}_3:\text{Yb}^{3+}(15 \text{ mol}\%)/\text{Er}^{3+}$ UCNPs for example) is provided in Fig. 3a, which shows that the as-prepared UCNPs possess a nearly

spherical shape. The large rings in the SAED pattern (Fig. 3b) are evidence of a polycrystalline structure. The structure of the UCNPs is further identified by high resolution TEM (HRTEM), as shown in Fig. 3c, which shows that the interplanar spacing of the nanocrystals is measured to be 0.317 nm, which further corresponds to the d value of the (111) crystallographic plane of monoclinic Gd_2O_3 ($d_{111} = 0.316$ nm, PDF#42-1465). The corresponding size distribution histogram (Fig. 3d) of UCNPs shows that the average size of the as-prepared UCNPs is approximately 7.8 nm. The XPS is employed to analyze the components of the samples. As shown in Fig. 4a, peaks at 1188.7 and 1220.4 eV denote $\text{Gd}3d_{5/2}$ and $\text{Gd}3d_{3/2}$, respectively, which are consistent with the reported results.^{37,38} The peaks at 141.0, 169.5, and 184.5 eV (Fig. 4b) denote $\text{Gd}4d$, $\text{Er}4d$, and $\text{Yb}4d$, respectively, which also match well with the previous reports.^{39,40} The peak intensity of the $\text{Yb}4d$ is enhanced with the increase in the Yb^{3+} concentration. The above XRD and XPS results demonstrate that $\text{Yb}^{3+}/\text{Er}^{3+}$ ions are co-doped in the Gd_2O_3 host matrix successfully.

Fig. 5 shows the UC fluorescence spectra of as-prepared $\text{Gd}_2\text{O}_3:\text{Yb}^{3+}$ (0–15 mol%)/ Er^{3+} UCNPs in the range of 400–750 nm, which were recorded under the same conditions. These UCNPs exhibit three emission bands in the visible range, including two green emissions and a red emission. The green emissions peaking at 528 and 547 nm originated from the ${}^2H_{11/2} \rightarrow {}^4I_{15/2}$ and ${}^4S_{3/2} \rightarrow {}^4I_{15/2}$ transitions of Er^{3+} ions, respectively, and the red emission (672 nm) comes from the ${}^4F_{9/2} \rightarrow {}^4I_{15/2}$ transition. Note that with the increase of Yb^{3+} concentration, the predominant emission for $\text{Gd}_2\text{O}_3:\text{Yb}^{3+}/\text{Er}^{3+}$ UCNPs shifts from the green band to red band. The corresponding

fluorescence images of the UCNPs (inserts in Fig. 5) and previous photographs of their colloids (Fig. 1b) depict visual evidence of the emission tuning process. The chromaticity coordinates were calculated from the UC emission spectra by the method using the 1931 CIE (Commission Internationale de l'Eclairage, France) system. As shown in Fig. 6, the calculated CIE chromaticity coordinates also reflect that the emission color shifts from the green region to the red region, and match well with their corresponding real fluorescence.

The UC process mainly proceeds via an excited state absorption (ESA) and an energy transfer upconversion (ETU).^{19,41} In the case of ESA, excitation takes the form of successive absorption of pump photons by the single activator ion. Fig. 7 displays the energy levels of Er^{3+} as well as the proposed UC mechanism of ESA in $\text{Gd}_2\text{O}_3:\text{Er}^{3+}$ (0 mol% Yb^{3+}) UCNPs. The 528, 547, and 672 nm emissions of Er^{3+} ions arise from the radiations of the ${}^2H_{11/2}$, ${}^4S_{3/2}$, and ${}^4F_{9/2}$ states, respectively. The ground state of Er^{3+} jump to the long-lived state via ground state absorption (GSA, ${}^4I_{15/2} \rightarrow {}^4I_{11/2}$), then populate ${}^4F_{7/2}$ state by ESA1 (${}^4I_{11/2} \rightarrow {}^4F_{7/2}$). Subsequently, the excited state (${}^4F_{7/2}$) relaxed to the ${}^2H_{11/2}/{}^4S_{3/2}$ state, from which the green emissions arises. Based on the energy gap law and experimental results, the multiphonon relaxation becomes competitive with the radiative decay when the gap is equal to or less than 4–5 times the phonon energy.^{28,42} Gd_2O_3 is a well-known host for efficient upconversion with small phonon energy ($\sim 600 \text{ cm}^{-1}$).³² The energy gap between the ${}^4F_{7/2}$ state and ${}^2H_{11/2}$ state is typically 1300 cm^{-1} , which means that the energy gap can be bridged by ~ 2 phonons. The nonradiative relaxation from ${}^4F_{7/2}$

to the next state (${}^2H_{11/2}$) is fast and radiative decay from the ${}^4F_{7/2}$ state cannot compete with multiphonon relaxation, thus no emission from the ${}^4F_{7/2}$ state is observed. After fast relaxation to the ${}^2H_{11/2}$ state, further nonradiative relaxation to the ${}^4S_{3/2}$ state, thus the low green emission (528 nm) from the ${}^2H_{11/2}$ state and intense green emission (547 nm) from the ${}^4S_{3/2}$ state are observed.

The ${}^4F_{9/2}$ state is generally considered to be populated by ESA2 (${}^4I_{13/2} \rightarrow {}^4F_{9/2}$) from the ${}^4I_{13/2}$ state, which arises from the nonradiative relaxation ($\sim 3620 \text{ cm}^{-1}$) of the ${}^4I_{11/2}$ state, or by nonradiative relaxation ($\sim 3080 \text{ cm}^{-1}$) from the ${}^4S_{3/2}$ state. The energy gaps of these two multiphonon relaxation processes need to be bridged by $\sim 5\text{--}6$ phonons; thus, relatively low red emission is found in Er^{3+} ions. In addition, the Cross Relaxation (CR) processes: ${}^4F_{7/2} \rightarrow {}^4F_{9/2}$ ($\sim 5190 \text{ cm}^{-1}$): ${}^4I_{11/2} \rightarrow {}^4F_{9/2}$ ($\sim 5030 \text{ cm}^{-1}$), among the Er^{3+} ions may take place due to the small energy mismatch, and contribute the population in the ${}^4F_{9/2}$ state.

The ETU mechanism dominates in the $\text{Yb}^{3+}\text{-Er}^{3+}$ co-doping system, due to the large absorption cross-section of Yb^{3+} in the NIR region than that of Er^{3+} . The essential difference between ETU and ESA is that the excitation in ETU is realized through energy transfer (ET) from nearby Yb^{3+} to Er^{3+} ions. Fig. 8a provides the energy levels of Yb^{3+} and Er^{3+} , as well as the proposed UC mechanism of ETU in $\text{Yb}^{3+}\text{-Er}^{3+}$ codoped Gd_2O_3 UCNPs. Under NIR excitation at 980 nm, the Yb^{3+} continuously absorbs 980 nm photons and transfers the energy to Er^{3+} to populate the ${}^2H_{11/2}$ (528 nm), ${}^4S_{3/2}$ (547 nm), and ${}^4F_{9/2}$ (672 nm) states. Since green emissions decrease with increasing Yb^{3+} concentration in $\text{Gd}_2\text{O}_3\text{:Yb}^{3+}/\text{Er}^{3+}$ UCNPs while the red

emission increases, the tuning mechanism responsible should be considered.

The CR process among the Er^{3+} ions and EBT from Er^{3+} to nearby Yb^{3+} ions have been found to have the ability to tune the intensity ratio of the red to green emission.^{31, 43} The CR (${}^4F_{7/2} \rightarrow {}^4F_{9/2} : {}^4I_{11/2} \rightarrow {}^4F_{9/2}$) process, which we have mentioned above, dramatically populates the ${}^4F_{9/2}$ state and contribute red emission. Wei et al. have obtained green to red fluorescence by utilizing the CR between Er^{3+} ions.²² The EBT process of ${}^4S_{3/2} \rightarrow {}^4I_{13/2}$ (Er^{3+} , $\sim 11730 \text{ cm}^{-1}$): ${}^2F_{7/2} \rightarrow {}^2F_{5/2}$ (Yb^{3+} , $\sim 10200 \text{ cm}^{-1}$) may readily take place due to a small energy mismatch ($\sim 1530 \text{ cm}^{-1}$), which can be made up by emission of ~ 3 phonons. Therefore, the ET from ${}^4S_{3/2}$ state of Er^{3+} to Yb^{3+} ions can be referred to the phonon-assisted EBT process.

According to Dexter's energy transfer theory, the probability of energy transfer has a $1/R^s$ dependence on the distance between two ions. Thus, the probability of CR ($P_{\text{Er} \leftrightarrow \text{Er}}$) and phonon-assisted EBT ($P_{\text{Er} \rightarrow \text{Yb}}$) from Er^{3+} to Yb^{3+} ions can be simplified as in Eqs. (1–2):⁴⁴

$$P_{\text{Er} \leftrightarrow \text{Er}} \propto 1/R_{\text{Er} \leftrightarrow \text{Er}}^s, \quad (1)$$

$$P_{\text{Er} \rightarrow \text{Yb}} \propto 1/R_{\text{Er} \leftrightarrow \text{Yb}}^s. \quad (2)$$

where $R_{\text{Er} \leftrightarrow \text{Er}}$ and $R_{\text{Er} \leftrightarrow \text{Yb}}$ are the average distances of Er^{3+} - Er^{3+} and Er^{3+} - Yb^{3+} , and s is a positive integer taking the values of 6, 8, and 10, which correspond to dipole-dipole, dipole-quadrupole, and quadrupole-quadrupole interactions, respectively. The $R_{\text{Er} \leftrightarrow \text{Er}}$ and $R_{\text{Er} \leftrightarrow \text{Yb}}$ can be expressed as in the following Eqs. (3–4):^{45, 46}

$$R_{\text{Er} \leftrightarrow \text{Er}} \approx 2 \left(\frac{3V}{4\pi C_{\text{Er}} N} \right)^{1/3}, \quad (3)$$

$$R_{Er \leftrightarrow Yb} \approx 2 \left(\frac{3V}{4\pi C_{Er+Yb} N} \right)^{1/3}. \quad (4)$$

where C_{Er} and C_{Er+Yb} are the doping concentration of the Er^{3+} ions, as well as the total doping concentration of Yb^{3+} and Er^{3+} ions, respectively. N is the number of available sites that the lanthanide ion can occupy in the unit cell, and V is the volume of the unit cell. In this work, we considered the effect of varying Yb^{3+} concentration on UC color tuning of $Gd_2O_3:Yb^{3+}/Er^{3+}$ UCNPs with Er^{3+} ions fixed at 2 mol%. The average Er^{3+} - Er^{3+} distance ($R_{Er \leftrightarrow Er}$) in the monoclinic Gd_2O_3 host is fixed, thus the effect of the R process can be neglected. The values of N and V are constants in one host while the $R_{Er \leftrightarrow Yb}$ decreases gradually with increasing the Yb^{3+} concentration, and the phonon-assisted EBT probability is enhanced (Fig. 8b). The phonon-assisted EBT process suppresses the population in the $^4S_{3/2}$ state and increase the population in the $^4I_{13/2}$ state. Further, the ET process of $^4I_{13/2} \rightarrow ^4F_{9/2} (Er^{3+})$; $^2F_{5/2} \rightarrow ^2F_{7/2} (Yb^{3+})$ effectively populates in the $^4F_{9/2}$ state. Thus, the phonon-assisted EBT process significantly enhances the red emission at 672 nm while it decreases the green emission.

To interpret the influence of a phonon-assisted EBT process on UC emission tuning, we introduced the following steady-state rate equations:

$$\frac{dP_4(t)}{dt} = P_{yb1}\omega_2P_2 - P_4R_4 - N_4\omega'P_{yb0} = 0, \quad (5)$$

$$\frac{dP_3(t)}{dt} = P_{yb1}\omega_1P_1 - P_3R_3 = 0, \quad (6)$$

$$\frac{dP_2(t)}{dt} = P_{yb1}\omega_0P_0 - P_2R_2 - P_{yb1}\omega_2P_2 = 0, \quad (7)$$

$$\frac{dP_1(t)}{dt} = N_4\omega'P_{yb0} - P_1R_1 - P_{yb1}\omega_1P_1 = 0, \quad (8)$$

$$\frac{dP_{Yb1}(t)}{dt} = I\sigma P_{Yb0}/h\nu + P_4\omega'P_{Yb0} - P_{Yb1}(\omega_0P_0 + \omega_1P_1 + \omega_2P_2) - RP_{Yb1} = 0. \quad (9)$$

where $P_0(\omega_0)$, $P_1(\omega_1, R_1)$, $P_2(\omega_2, R_2)$, $P_3(\omega_3, R_3)$, and $P_4(\omega_4, R_4)$ are the population densities (ET rates from excited Yb³⁺ ions, radiation rates) of the $^4I_{15/2}$, $^4I_{13/2}$, $^4I_{11/2}$, $^4F_{9/2}$, and $^4S_{3/2}$ states (Er³⁺), respectively. P_{Yb0} and P_{Yb1} are the population densities of the ground state and excited state in Yb³⁺ ions, respectively. ω' is the phonon-assisted EBT rate from Er³⁺ to Yb³⁺ ions, I is the excitation intensity and ν is the laser frequency, σ is the absorption cross section of Yb³⁺ ions, and the R is the radiation rate of the $^2F_{5/2}$ state (Yb³⁺).

The UC rates $P_{Yb1}\omega_1P_1$, $P_{Yb1}\omega_2P_2$ dominate and the linear decays P_1R_1 , P_2R_2 generally can be neglected in Eqs. (5–6). Doping with no Yb³⁺ ions (for Gd₂O₃:Er³⁺ UCNPs), the linear decay R_4 is dominated without the phonon-assisted EBT. Thus, we have $P_1=0$, $P_2=\omega_0P_0/\omega_2$, $P_3=0$, and $P_4=\omega_0P_0P_{Yb1}/R_4$, which means the green emission is dominated in Gd₂O₃:Er³⁺ UCNPs. In the Er³⁺-Yb³⁺ co-doping system, the phonon-assisted EBT rate ω' cannot be neglected. The following relationships between the steady-state population densities (P_1 , P_2 , P_3 , and P_4) and phonon-assisted EBT rate (ω') are obtained from Eqs. (5–8):

$$P_4 = \omega_0P_0P_{Yb1}/(R_4 + \omega'P_{Yb0}), \quad (10)$$

$$P_3 = \omega_0\omega'P_0P_{Yb0}P_{Yb1}/R_3(R_4 + \omega'P_{Yb0}), \quad (11)$$

$$P_2 = \omega_0P_0/\omega_2, \quad (12)$$

$$P_1 = \omega_0\omega'P_0P_{Yb0}/\omega_1(R_4 + \omega'P_{Yb0}). \quad (13)$$

P_1 and P_3 are the strictly increasing functions of ω' , while P_4 is a monotone decreasing function. At very high Yb³⁺ ions concentrations, the phonon-assisted EBT

rate ω' is dominated and the linear decay R_4 can be neglected. Thus, we get:

$$P_4 = \omega_0 P_0 P_{Yb1} / \omega' P_{Yb0} \approx 0, \quad (14)$$

$$P_3 = \omega_0 P_0 P_{Yb1} / R_3, \quad (15)$$

$$P_1 = \omega_0 P_0 / \omega_1. \quad (16)$$

Note that the P_{Yb0} is much larger than P_{Yb1} , and therefore P_4 can be neglect compared with P_3 , which indicates that the green emission can be greatly decreased and the red emission can be enhanced when the phonon-assisted EBT is highly efficient. These results agree well with the above experimental data. Due to the phonon-assisted EBT, the intensity ratio of the red to green emission gradually increases with increasing Yb^{3+} concentration, so that the real fluorescence color is continuously adjusted.

3. Experimental section

3.1 Materials

All reagents were of analytical grade without further purification. Gd_2O_3 , Yb_2O_3 , and Er_2O_3 powder (99.99%) were purchased from Aladdin Chemistry Co. Ltd. The Deionized water without further purification is used.

3.2 Syntheses

We synthesized the $\text{Gd}_2\text{O}_3:\text{Yb}^{3+}/\text{Er}^{3+}$ UCNPs by adopting tow-steps, which combine LAL with a standard solid state reaction technique. The details were reported in our previous work.³⁴⁻³⁶ First, $\text{Gd}_2\text{O}_3:\text{Yb}^{3+}/\text{Er}^{3+}$ bulk targets were prepared by a standard solid-state reaction technique. Then, the prepared targets were fixed on the

bottom of the container and immersed in deionized water, and a microsecond Nd:YAG laser with a wavelength of 1064 nm, 6 μ s pulse duration, repetition of 100 Hz, and power of 70 mJ/pulse, was focused onto the surface of the bulk targets. The ablation process lasted 15 min. The ablated colloids were aged for 24 h; then, the upper aqueous suspension was collected for further measurement.

3.3 Characterization

One drop of the aqueous suspension was placed on a carbon coated copper grid, and the sample was observed using a transmission electron microscope (TEM, FEI Tecnai G2 Spirit, Netherlands) operating at 120 kV. A histogram of the particles size distribution was constructed by measuring the particles (249 in total) in the TEM image. The samples for XRD, XPS, and fluorescence spectra measurements were prepared as follows. Several drops of aqueous suspension were placed on a silicon wafer, and dried at 50 °C. This process was repeated several times until a thin white layer was formed. The crystalline structure of the samples was measured by using an X-ray diffractometer (XRD, D-MAX2200 VPC, Japan) with Cu-K α radiation at 46 kV and 26 mA, and 2θ ranging from 25° to 65°. The chemical compositions of the nanoparticles were determined via X-ray photoelectron spectrometry (XPS, ESCALab250, USA). The fluorescence spectrum of the UCNPs was recorded by a combined lifetime and steady state fluorescence spectrometer (FLS920, UK) at room temperature, equipped with a 980 nm laser.

4. Conclusion

We investigated the sensitizer (Yb^{3+}) concentration dependent UC fluorescence in ultra-small (sub-10 nm) $\text{Gd}_2\text{O}_3:\text{Yb}^{3+}/\text{Er}^{3+}$ UCNPs. An enhancement of phonon-assisted EBT from Er^{3+} to nearby Yb^{3+} ions can be induced by increasing the Yb^{3+} doping concentration. This process is directly suppressed in the green emission but is enhanced in the red emission. By harnessing this important feature, we precisely manipulate the UC color output (from green to red) by slightly increasing the Yb^{3+} ion concentration (from 0 to 15 mol%) in the $\text{Gd}_2\text{O}_3:\text{Yb}^{3+}/\text{Er}^{3+}$ UCNPs. These results show the potential application of the $\text{Gd}_2\text{O}_3:\text{Yb}^{3+}/\text{Er}^{3+}$ UCNPs as fluorescence nanoprobes in multiplexed bioimaging.

Acknowledgment

This work was supported by the National Basic Research Program of China (2014CB931700), the National Natural Science Foundation of China (Grant Nos.81471787, 61471401 and 11274394), the Natural Science Foundation of Guangdong Province (Grant No. S2012010010542).

Notes and references

1. F. Wang, Y. Han, C. S. Lim, Y. Lu, J. Wang, J. Xu, H. Chen, C. Zhang, M. Hong and X. Liu, *Nature*, 2010, 463, 1061-1065.
2. G. Chen, J. Shen, T. Y. Ohulchanskyy, N. J. Patel, A. Kutikov, Z. Li, J. Song, R. K. Pandey, H. Ågren, P. N. Prasad and G. Han, *ACS Nano*, 2012, 6, 8280-8287.
3. L. Cheng, C. Wang and Z. Liu, *Nanoscale*, 2013, 5, 23-37.
4. H. Kobayashi, Y. Hama, Y. Koyama, T. Barrett, C. A. S. Regino, Y. Urano and P.

- L. Choyke, *Nano Lett.*, 2007, 7, 1711-1716.
5. L. Cheng, K. Yang, S. Zhang, M. Shao, S. Lee and Z. Liu, *Nano Res.*, 2010, 3, 722-732.
6. H. S. Mader, P. Kele, S. M. Saleh and O. S. Wolfbeis, *Curr. Opin. Chem. Biol.*, 2010, 14, 582-596.
7. G. Chen, T. Y. Ohulchanskyy, S. Liu, W.-C. Law, F. Wu, M. T. Swihart, H. Ågren and P. N. Prasad, *ACS nano*, 2012, 6, 2969-2977.
8. S. Wu, N. Duan, Z. Shi, C. Fang and Z. Wang, *Anal. Chem.*, 2014, 86, 3100-3107.
9. B. A. Smith, B.-W. Xie, E. R. van Beek, I. Que, V. Blankevoort, S. Xiao, E. L. Cole, M. Hoehn, E. L. Kaijzel, C. W. G. M. Löwik and B. D. Smith, *ACS Chem. Neurosci.*, 2012, 3, 530-537.
10. J. Pecher, J. Huber, M. Winterhalder, A. Zumbusch and S. Mecking, *Biomacromolecules*, 2010, 11, 2776-2780.
11. M. Wang, C. Mi, Y. Zhang, J. Liu, F. Li, C. Mao and S. Xu, *J. Phys. Chem. C*, 2009, 113, 19021-19027.
12. W. Zheng, S. Zhou, Z. Chen, P. Hu, Y. Liu, D. Tu, H. Zhu, R. Li, M. Huang and X. Chen, *Angew. Chem. Int. Ed.*, 2013, 52, 6671-6676.
13. D. Gao, X. Zhang, H. Zheng, P. Shi, L. Li and Y. Ling, *Dalton. Trans.*, 2013, 42, 1834-1841.
14. S. Ye, G. Chen, W. Shao, J. Qu and P. N. Prasad, *Nanoscale*, 2015, 7, 3976-3984.
15. F. Wang, R. Deng, J. Wang, Q. Wang, Y. Han, H. Zhu, X. Chen and X. Liu, *Nat.*

- Mater.*, 2011, 10, 968-973.
16. J. Wang, F. Wang, C. Wang, Z. Liu and X. Liu, *Angew. Chem. Int. Ed.*, 2011, 50, 10369-10372.
 17. G. Chen, H. Liu, G. Somesfalean, H. Liang and Z. Zhang, *Nanotechnology*, 2009, 20, 385704.
 18. W. Gao, H. Zheng, Q. Han, E. He, F. Gao and R. Wang, *J. Mater. Chem. C*, 2014, 2, 5327-5334.
 19. F. Auzel, *Chem. Rev.*, 2004, 104, 139-174.
 20. J. Wang, R. Deng, M. A. MacDonald, B. Chen, J. Yuan, F. Wang, D. Chi, T. S. A. Hor, P. Zhang and G. Liu, *Nat. Mater.*, 2013, 13, 157-162.
 21. F. Wang and X. Liu, *Chem. Soc. Rev.*, 2009, 38, 976-989.
 22. W. Wei, Y. Zhang, R. Chen, J. Goggi, N. Ren, L. Huang, K. K. Bhakoo, H. Sun and T. T. Y. Tan, *Chem. Mater.*, 2014, 26, 5183-5186.
 23. F. Wang and X. Liu, *J. Am. Chem. Soc.*, 2008, 130, 5642-5643.
 24. G. Chen, H. Qiu, R. Fan, S. Hao, S. Tan, C. Yang and G. Han, *J. Mater. Chem.*, 2012, 22, 20190-20196.
 25. D. Chen, Y. Zhou, Z. Wan, H. Yu, H. Lu, Z. Ji and P. Huang, *Phys. Chem. Chem. Phys.*, 2015, 17, 7100-7103.
 26. A. Newport, G. R. Fern, T. Ireland, R. Withnall, J. Silver and A. Vecht, *J. Mater. Chem.*, 2001, 11, 1447-1451.
 27. F. Vetrone, J.-C. Boyer, J. A. Capobianco, A. Speghini and M. Bettinelli, *J. Appl. Phys.*, 2004, 96, 661-667.

28. H. Guo, N. Dong, M. Yin, W. Zhang, L. Lou and S. Xia, *J. Phys. Chem. B*, 2004, 108, 19205-19209.
29. Y. Lei, H. Song, L. Yang, L. Yu, Z. Liu, G. Pan, X. Bai and L. Fan, *J. Chem. Phys.*, 2005, 123, 174710-174710.
30. G. Y. Chen, Y. G. Zhang, G. Somesfalean, Z. G. Zhang, Q. Sun and F. P. Wang, *Appl. Phys. Lett.*, 2006, 89, 163105.
31. V. M. Lojpur, P. S. Ahrenkiel and M. D. Dramićanin, *Nanoscale. Res. Lett*, 2013, 8, 1-6.
32. K. Zheng, D. Zhang, D. Zhao, N. Liu, F. Shi and W. Qin, *Phys. Chem. Chem. Phys.*, 2010, 12, 7620-7625.
33. L. Zhou, Z. Gu, X. Liu, W. Yin, G. Tian, L. Yan, S. Jin, W. Ren, G. Xing and W. Li, *J. Mater. Chem.*, 2012, 22, 966-974.
34. J. Liu, X. Tian, H. Chen, Y. Shao, G. Yang and D. Chen, *Appl. Surf. Sci.*, 2014, doi:10.1016/j.apsusc.2014.1011.1105.
35. J. Liu, X. Tian, N. Luo, C. Yang, J. Xiao, Y. Shao, X. Chen, G. Yang, D. Chen and L. Li, *Langmuir*, 2014, 30, 13005-13013.
36. N. Q. Luo, C. Yang, X. M. Tian, J. Xiao, J. Liu, F. Chen, D. H. Zhang, D. K. Xu, Y. L. Zhang, G. W. Yang, D. H. Chen and L. Li, *J. Mater. Chem. B*, 2014, 2, 5891-5897.
37. D. Raiser and J. P. Deville, *J. Electron. Spectrosc. Relat. Phenom.*, 1991, 57, 91-97.
38. D. Sarma and C. Rao, *J. Electron. Spectrosc. Relat. Phenom.*, 1980, 20, 25-45.

39. Y. Zhang, R.-Z. Wang, S.-G. Xiao, M.-H. Qu, K.-Y. Li, C.-X. Liu, X.-F. Wang, X.-H. Yan and H. Yan, *J. Lumin.*, 2014, 145, 351-356.
40. T. Miyazaki, R. Sumii, H. Umemoto, H. Okimoto, Y. Ito, T. Sugai, H. Shinohara, T. Zaima, H. Yagi and S. Hino, *Chem. Phys.*, 2012, 397, 87-91.
41. M. Haase and H. Schäfer, *Angew. Chem. Int. Ed.*, 2011, 50, 5808-5829.
42. L. Aarts, B. Van der Ende and A. Meijerink, *J. Appl. Phys.*, 2009, 106, 023522.
43. L. Shi, Q. Shen and Z. Qiu, *J. Lumin.*, 2014, 148, 94-97.
44. D. L. Dexter, *The Journal of Chemical Physics*, 1953, 21, 836-850.
45. Y. Huang, H. You, G. Jia, Y. Song, Y. Zheng, M. Yang, K. Liu and N. Guo, *J. Phys. Chem. C*, 2010, 114, 18051-18058.
46. D. Yang, G. Li, X. Kang, Z. Cheng, P. a. Ma, C. Peng, H. Lian, C. Li and J. Lin, *Nanoscale*, 2012, 4, 3450-3459.

Figure Captions

Figure 1 (a) Schematic illustration of the UC process for UCNPs under NIR excitation. (b) Digital UC fluorescence images of the $\text{Gd}_2\text{O}_3:\text{Yb}^{3+}(0-15 \text{ mol } \%)/\text{Er}^{3+}$ UCNPs colloids under excitation at 980 nm (no optical filters were used).

Figure 2 XRD patterns of the $\text{Gd}_2\text{O}_3:\text{Yb}^{3+}(0-15 \text{ mol } \%)/\text{Er}^{3+}$ UCNPs, compared to PDF#42-1465 for monoclinic Gd_2O_3 .

Figure 3 (a) Typical TEM, (b) SAD pattern, (c) HRTEM, and (d) Size distribution histogram of the $\text{Gd}_2\text{O}_3:\text{Yb}^{3+}(15 \text{ mol } \%)/\text{Er}^{3+}$ UCNPs.

Figure 4 Gd3d, Gd4d, Yb4d, and Er4d XPS spectra of $\text{Gd}_2\text{O}_3:\text{Yb}^{3+}(0-15 \text{ mol } \%)/\text{Er}^{3+}$

UCNPs.

Figure 5 Room temperature UC emission spectra of the $\text{Gd}_2\text{O}_3:\text{Yb}^{3+}$ (0–15 mol %)/ Er^{3+} UCNPs under 980 nm excitation.

Figure 6 CIE chromaticity diagram showing the color coordinates of the $\text{Gd}_2\text{O}_3:\text{Yb}^{3+}$ (0–15 mol %)/ Er^{3+} UCNPs.

Figure 7 Energy-level diagram of the Er^{3+} ions and proposed UC mechanism schemes of the $\text{Gd}_2\text{O}_3:\text{Er}^{3+}$ UCNPs.

Figure 8 Energy-level diagram of the Er^{3+} and Yb^{3+} ions and proposed UC mechanism schemes of the $\text{Gd}_2\text{O}_3:\text{Yb}^{3+}/\text{Er}^{3+}$ UCNPs.

Figure 1

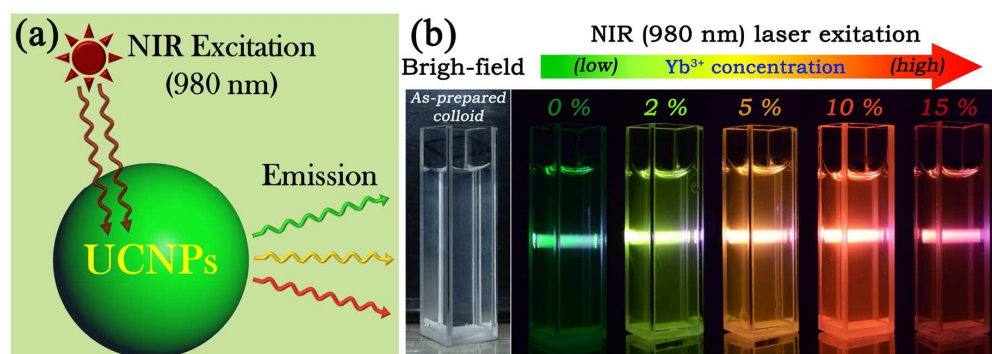


Figure 2

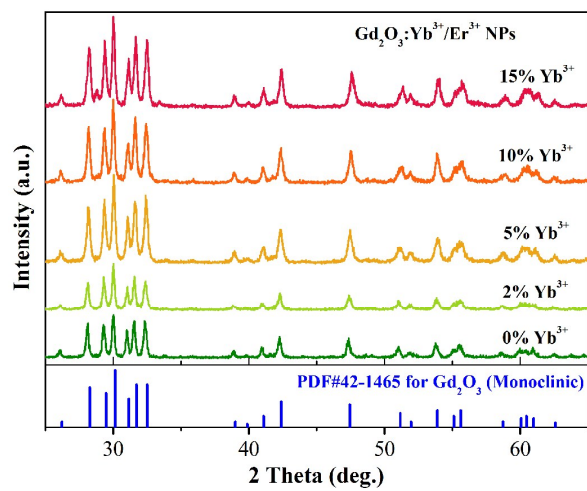


Figure 3

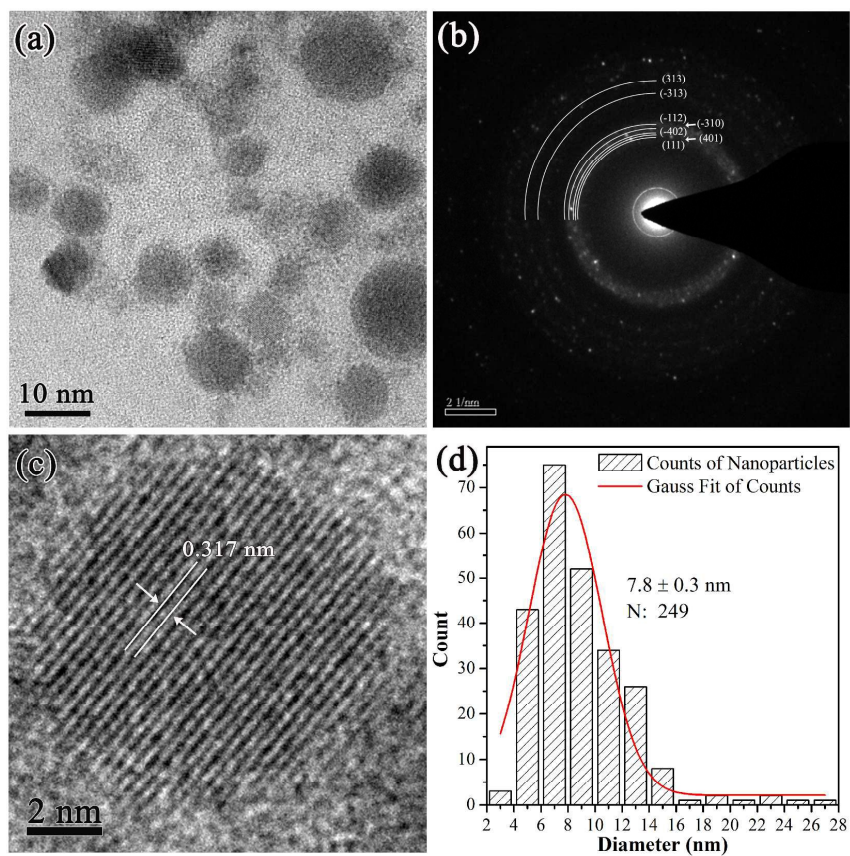


Figure 4

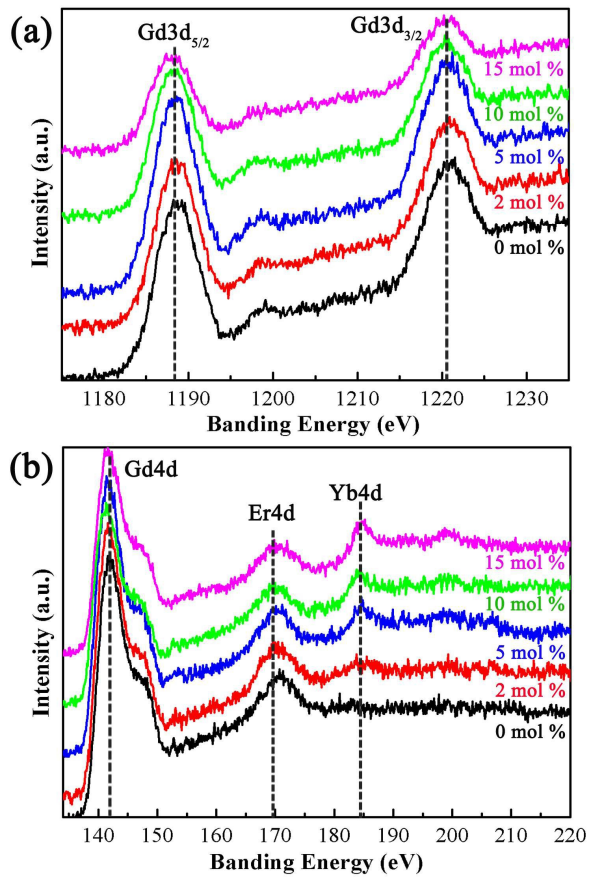


Figure 5

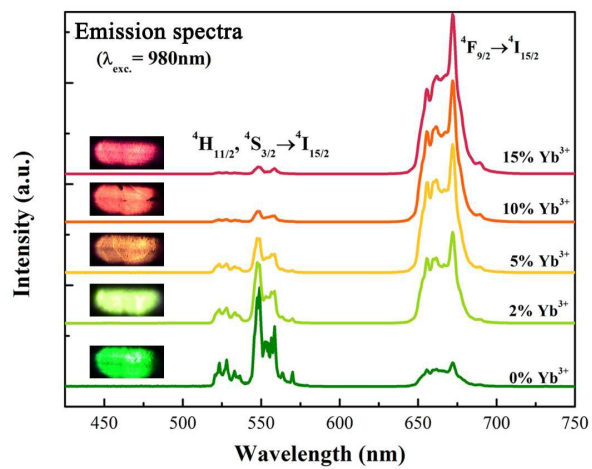


Figure 6

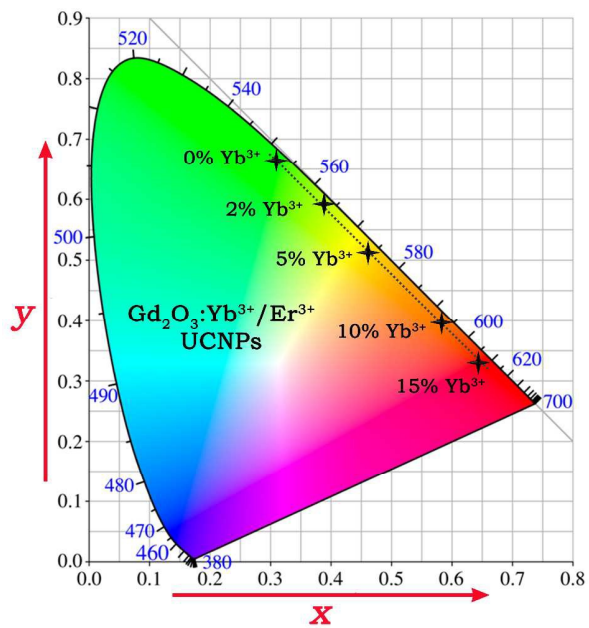


Figure 7

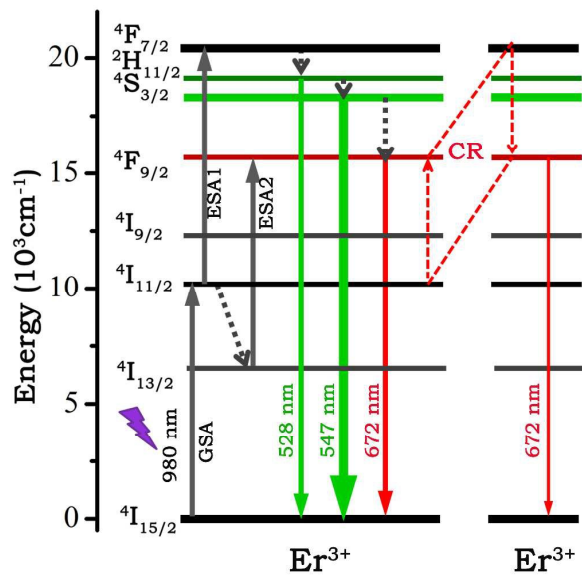


Figure 8

